

Segmentation of Optic Disc and Blood Vessels in Retinal Images using Wavelets, Mathematical Morphology and Hessian-based Multi-scale Filtering

Luiz Carlos Rodrigues and Maurício Marengoni

Department of Electrical Engineering, Universidade Presbiteriana Mackenzie, São Paulo, Brazil

Keywords: Retinal Images, Mathematical Morphology, Wavelets, Multi-scale Filter.

Abstract: A digitized image captured by a fundus camera provides an effective, inexpensive and non-invasive resource for the assessment of vascular damage caused by diabetes, arterial hypertension, hypercholesterolemia and aging. These unhealthy conditions may have very serious consequence like hemorrhages, exudates, branch retinal vein occlusion, leading to the partial or total loss of vision capabilities. This study has focus on the computer vision techniques of image segmentation required for a completely automated assessment system for the vascular conditions of the eye. The study here presented proposes a new algorithm based on wavelets transforms and mathematical morphology for the segmentation of the optic disc and a Hessian based multi-scale filtering to segment the vascular tree in color eye fundus photographs. The optic disc and vessel tree, are both essential to the analysis of the retinal fundus image. The optic disc can be identified by a bright region on the fundus image, for its segmentation we apply Haar wavelets transform to obtain the low frequencies representation of the image and then apply mathematical morphology to enhance the segmentation. The tree vessel segmentation is achieved using a Hessian-based multi-scale filtering that, based on its second order derivatives, explores the tubular shape of a blood vessel to classify the pixels as part, or not, of a vessel. The proposed method is being developed and tested based on the DRIVE database, which contains 40 color eye fundus images.

1 INTRODUCTION

The automated retinal image analysis has become, during the recent years, a large field of research due the advances in computer vision techniques and image acquisition. This growing interest is due to several factors outlined below (Rossant et al., 2011):

1. Eye fundus is the only location of the human body where the blood vessels can be visualized non-invasively *in vivo*.
2. Retinal images can be produced, distributed and processed in a relatively inexpensive way.
3. Retinal vessels and arteries are strong and trustable indicators of pathologies as diabetes, arterial hypertension and high level of cholesterol.

Beyond the context of the clinical research, automated methods of retinal images analysis have a social high importance since they create the possibility to realize very quickly exams in a large number of images, saving time and human resources and still offering more quantitative metrics than the human observation

techniques. The proposed method was developed and tested on the DRIVE (Digital Retinal Images for Vessel Extraction) database, which contains 40 color eye fundus images. Each image is captured using 8 bits per color plane and has the size of 593 x 576 pixels. The FOV of each image is circular with a diameter of approximately 540 pixels. For research reference, manual segmentations are also available and have been performed by three independent observers. The database is decomposed in a training set of 20 images and a test set of 20 images (Staal et al., 2004).

1.1 Related Works

Many researches have been developed and were related by (Fraz et al., 2012). Algorithms and methodologies for detecting retinal blood vessels can be grouped into techniques based on pattern recognition, wavelets, morphological processing, matching filtering, vessel tracking, and model-based algorithms. The pattern recognition algorithm can be subdivided in two branches: supervised methods and unsuper-

vised methods. Supervised methods utilizes ground truth data for the classification of vessels based on a given vector of characteristics. These methods include neural network (Marín et al., 2010), principal component analysis (Sinthanayothin et al., 1999), k-nearest neighbor classifier and ridge based primitives classification (Staal et al., 2004), support vector machine (SVM) classification (Ricci and Perfetti, 2007) and feature-based Adaboost classifier (Lupas et al., 2010). The unsupervised methods work without having any prior labeling knowledge, and do not have a previous training phase. Some reported methods are fuzzy C-means clustering algorithm, radius-based clustering algorithm, maximum likelihood estimation of vessel parameters, matched filtering along with specially weighted fuzzy C-means clustering (Kande et al., 2010).

2 THEORETICAL BACKGROUND

2.1 Wavelets Transform (WT)

The wavelet transform is a signal decomposition as a combined basis functions set, obtained by dilation (a) and translations (b) of a single prototype wavelet $\psi(t)$. Thus, the WT of a signal $x(t)$ is defined as

$$W(a, b) = \int_{-\infty}^{+\infty} f(t) \frac{1}{\sqrt{|a|}} \psi^* \left(\frac{t-b}{a} \right) dt \quad (1)$$

The greater the scale factor a is, the wider is the basis function and consequently, the corresponding coefficients gives information about lower frequency components of the signal, and vice versa. In this way, the temporal resolution is higher at high frequencies, achieving the property that the analysis window comprises the same number of periods for any central frequency. If the prototype wavelet $\psi(t)$ is the derivative of a smoothing function $\theta(t)$, it can be shown (Burrus et al., 1998) that the wavelet transform of a signal $x(t)$ at scale a is:

$$W(a, b) = \int_{-\infty}^{+\infty} f(t) \frac{1}{\sqrt{|a|}} \psi^* \left(\frac{t-b}{a} \right) dt \quad (2)$$

where $\theta(t) = \left(\frac{1}{\sqrt{a}} \theta \frac{t}{a} \right)$ is the scaled version of the smoothing function. The wavelet transform at scale a is proportional to the derivative of the signal filtered version with a smoothing impulse response at scale a . Therefore the zero crossing of the WT corresponds to the local maxima or minima of the smoothed signal at different scales and the maximum absolute values of the wavelet transforms are associated with maximum slopes in the filtered signal. In this study we

are interested in images processing which are composed of slopes and local maxima (or minima) at different scales occurring at different level of intensity of the pixels. The scale factor a or the translation parameter b can be discretized. The usual choice is to follow a dyadic grid on the time-scale plane: $a = 2^k$ and $b = 2^k l$. This transform is called *dyadic wavelet transform* with basis functions (Addison, 2005)

$$\psi_{k,l}(t) = 2^{(-\frac{k}{2})} \psi(2^k t - l) \text{ where } k, l \in \mathbf{Z}^+ \quad (3)$$

For discrete-time signals, the dyadic discrete wavelet transform (DWT) is equivalent, according to Mallat's algorithm (Mallat, 1989), to an octave filter bank and can be implemented as a cascade of identical cells, low-pass and high-pass finite impulse response [FIR] filters, as illustrated in Fig. 1. From the transformed coefficients $W_{2^k x}[2^k l]$ and the low-pass residual, the original sign can be rebuilt using a reconstruction filter bank. The down samplers after each filter in Fig.1 remove the redundancy of the signal representation. As side effects, they make the signal representation time variant and reduce the temporal resolution of the wavelet coefficient for increasing scales.

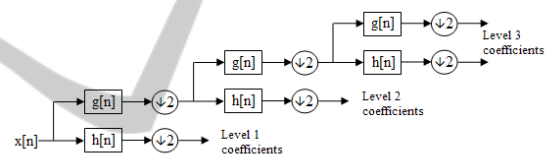


Figure 1: Mallat's algorithm for the two filter bank implementation of DWT.

2.2 Mathematical Morphology

The word *morphology* refers to form and structure; in computer vision it can be used to refer to the shape of a region. The operations of *mathematical morphology* were originally defined as set operations and shown to be useful for processing sets of 2D points (Shapiro and Stockman, 2001). The language of mathematical morphology is the set theory. Sets in mathematical morphology represent the shapes which are represented in binary or gray tone. The set of all black pixels in a black white image, a binary image constitutes a complete description of the binary image (Haralick and Sternberg, 1987). The operations of binary morphology input a binary image \mathbf{B} and a structuring element \mathbf{S} , usually another smaller binary image. The structuring element represents a shape; it can have an arbitrary size.

2.3 Scale-Space and Hessian-based Filtering

The scale-space theory is a framework conceived for the representation of an image, or signal, in multiple scales, or apertures (Witkin, 1983). Its motivation comes from the resemblance of close receptive field profiles of human visual system and intends the representation of an object in multiple scales simultaneously, obeying some axioms like linearity, spacial shift invariance, isotropy and scale invariance (Florack et al., 1992). Based on scale-spaces theory (Koenderink, 1984), Frangi et al. (Frangi et al., 1998) developed a multi scale approach to the use of the eigenvalues of the Hessian to determine locally the likelihood that a pixel may be considered a part of a vessel. This conceives the vessel enhancement as a filtering process that searches for geometrical structures which may be considered a tubular shape. The idea is, given a point \mathbf{x}_0 in an image, to consider the Taylor expansion in its neighbourhood,

$$L(x_0 + \delta x_0, s) \approx L(x_0 + x_0, s) + \delta x_0^T \Delta_{0,s} + \delta x_0^T H_{0,s} \delta x_0 \quad (4)$$

Where $\Delta_{0,s}$ is the gradient vector and H represents the Hessian matrix, a 2-by-2 matrix containing the second partial derivatives of a function, as shown for a 2D image $I(x, y)$ in (5) The Hessian matrix contains also all the second order information needed for each pixel. To extract information about contrast and direction of a pixel from the Hessian matrix its eigenvalues are calculated.

$$\mathbf{H}(x, y) = \begin{pmatrix} \frac{\partial^2 I}{\partial x^2} & \frac{\partial^2 I}{\partial x \partial y} \\ \frac{\partial^2 I}{\partial x \partial y} & \frac{\partial^2 I}{\partial y^2} \end{pmatrix} \quad (5)$$

Like the image I , the Hessian is also a discrete function and may be approximated to a continuous function using the 2-dimensional Gaussian (6) filter and the convolution differentiation property according (7)

$$\mathbf{G}(x, y) = e^{-\frac{1}{2}(\frac{x^2}{\sigma_1^2} + \frac{y^2}{\sigma_2^2})} \quad (6)$$

$$\mathbf{H}(x, y) \approx G * \begin{pmatrix} \frac{\partial^2 I}{\partial x^2} & \frac{\partial^2 I}{\partial x \partial y} \\ \frac{\partial^2 I}{\partial x \partial y} & \frac{\partial^2 I}{\partial y^2} \end{pmatrix} = \begin{pmatrix} \frac{\partial^2 G}{\partial x^2} & \frac{\partial^2 G}{\partial x \partial y} \\ \frac{\partial^2 G}{\partial x \partial y} & \frac{\partial^2 G}{\partial y^2} \end{pmatrix} * \mathbf{I}(x, y), \quad (7)$$

where $*$ is the convolution symbol. Let $|\lambda_1| \leq |\lambda_2|$ represent the two eigenvalues calculated from the Hessian matrix and \mathbf{u}_1 and \mathbf{u}_2 the correspondent eigenvectors. Since $|\lambda_1|$ is the eigenvalue of smallest magnitude it corresponds to the eigenvector, \mathbf{u}_1 ,

pointing out the direction of smallest curvature, and $|\lambda_2|$ corresponds to the eigenvector \mathbf{u}_2 pointing out the direction of largest curvature. In terms of a blood vessel, it means that \mathbf{u}_1 is parallel to longitudinal axis of the blood vessel, and $|\lambda_1| \cong 0$ while \mathbf{u}_2 is parallel to the radial axis. With these values, two measures were created to assess the anisotropy and the contrast of the pixel. These measures are obtained by (8) and (9).

$$\mathbf{R}_a = \frac{|\lambda_1|}{|\lambda_2|} \quad (8)$$

$$\mathbf{R}_b = \sqrt{|\lambda_1|^2 + |\lambda_2|^2} \quad (9)$$

During the process of classification of a given pixel, the lower R_a higher is the probability of the pixel be part of a vessel.

R_b will be low if both eigenvalues are small for the lack of contrast so that larger R_b higher is the probability of the pixel be part of a vessel.

For images where the vessels are darker than their background, what means that these vessels are represented like valleys, the curvature will be negative so $|\lambda_2| < 0$.

These conclusions led the development of a likelihood function, also known as "vesselness equation"(10) at each scale s ,

$$V_0(s) = \begin{cases} 0 & \text{if } \lambda_2 > 0 \\ e^{-\frac{R_a^2}{2\alpha^2}} (1 - e^{-\frac{R_b^2}{2\beta^2}}) & \text{otherwise} \end{cases} \quad (10)$$

where α and β are thresholds which control the sensitivity of the line filter to the measures R_a and R_b .

The table 1 illustrates the possible patterns assumed by the combination of the ordered eigenvalues ($|\lambda_1| < |\lambda_2|$) for a 2D image.

Table 1: Possible patterns in 2D depending on the value of the eigenvalues λ_k . +/- indicate the sign of the eigenvalues.

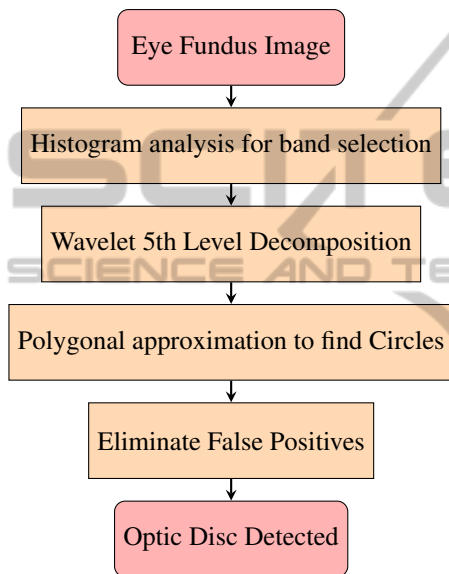
Eigenvalues		Orientation Pattern
λ_1	λ_2	
Noisy	Noisy	noisy, no preferred direction
Low	High-	tubular structure (bright)
Low	High+	tubular structure (dark)
High-	High-	blob-like structure (bright)
High+	High+	blob-like structure (dark)

3 METHODS

3.1 Optic Disc Segmentation

In this section we describe the process to extract the localization of the optic disc analyzing the eye fundus

image provided by DRIVE database. The optic disc is the region of entrance of the blood vessels and the optic nerve into the retina. The appearance of the optic disc in a color fundus image is a bright yellowish or white region. Its contour is more or less circular and it is interrupted by the outgoing vessels. Non rare it may have an elliptical form due the considerable angle between the image plane and the object plane. The diameter may assume different sizes depending on the patient and is in the range of 40 to 60 pixels in 640 x 480 color images. The complete algorithm is represented by the diagram shown in the flowchar below.



We first read an JPG image of DRIVE image and execute an Histogram Analysis, comparing with three reference images that will indicate the best color band to consider for processing. Each of our three image reference is associated to the selection of one of the three color bands. Higher the level of histogram similarity of the input image with one of image reference, the image reference will indicate the best band to be processed, discarding the others two. These three image reference were selected based in empirical testings. The reason for this procedure is that not always a selected color band is good enough for processing the all set of samples, since each sample may presents very different distribution of gray scales, increasing the error of the algorithm. As shown in Fig. 2 for the first test record, the upper picture, the more suitable band to locate the optic disc in Red band, due the good contrast. However, for second test record, shown below, the best option would be the green band, once the Red band has a very low contrast, increasing the difficulties to locate the optic disc. Once selected, the best band is submitted to an pyramidal Haar wavelet

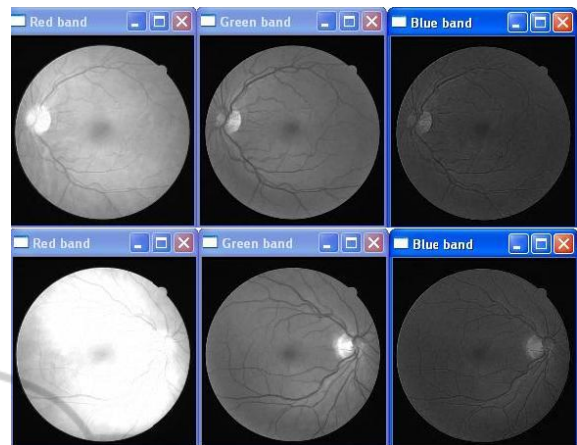


Figure 2: Above the RGB bands of the first record of set test set. Below the RGB bands of the second record of the test set.

decomposition that produce a sub bands vector, containing the frequencies approximations of the image. The 5th level of decomposition with 37x36 pixels is then resized and interpolated to an original size of the image, 592 x 576. We then convert the interpolated 5th level wavelets approximation into a binary image, applying a threshold of minimum pixel value of 220 and a maximum pixel value of 225. The result is show in Fig. 3

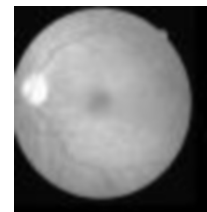


Figure 3: Example of the 5th level of wavelet transform signal decomposition.

3.2 Retinal Vessel Segmentation

The multi-scale vessel detection was performed for scales between t_{min} and t_{max} (corresponding to σ_{min} to σ_{max}). For each $\sigma \in \langle \sigma_{min}; \sigma_{max} \rangle$ the Hessian matrices were calculated using (7). The the eigenvalue analysis was performed using the criteria described in Section 2.3 and the results for each scale were obtained. The final result of the multi-scale analysis pixel-wise maximum of obtained results over all analyzed scales.

4 EXPERIMENTAL RESULTS

4.1 Optic Disc Segmentation

The 20 color images of the DRIVE database were submitted to this algorithm. In 17 images, the optic disc was correctly localized. And in 10 images the exact contour was also found. However, due the low contrast we found some false positives and in two images the algorithm failed and the result was not acceptable. As a initial result it maybe considered a good outcome, since the bad results are consequence of abnormal optic disk that require an additional pre-processing on the image. This pre-processing is under elaboration and we intend to implement it and improve significantly the process.

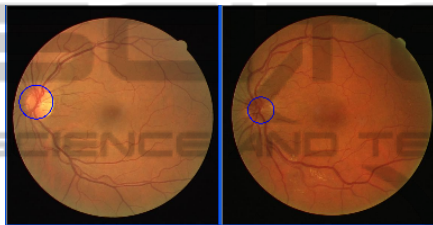


Figure 4: Two examples of optic disc outlines determined by this method.

4.2 Retinal Vessel Segmentation

The green channel of the RGB-colored retinal image was selected for the image processing because it normally presents a better contrast between the blood vessels and the retinal background. DRIVE database image makes available a binary mask for the FOV for each record. The 20 images of DRIVE database were used to assess this algorithm. We use these masks as reference to determine the accuracy of our algorithm. The first results are fully satisfactory and we obtained good results in images with high and low contrast. Smaller vessels that are not connected to the vascular tree might be missed without prejudice to the purpose of this study.

Fig. 6 shows an example of a blood vessel segmentation of a green channel. The two examples are a result of a empirical test, when we processed the image until the sixth scale, starting with $\sigma = 0.5$, with increments of 0.3 and $R_a = 2$ and $R_b = 10$.

Several studies have been made on blood vessel segmentation using the DRIVE database. Some of these studies are shown in the table 2:

Comparing with the other studies, it is remarkable the average accuracy achieved by the implementation of Hessian-based multi-scale filter without any pre-

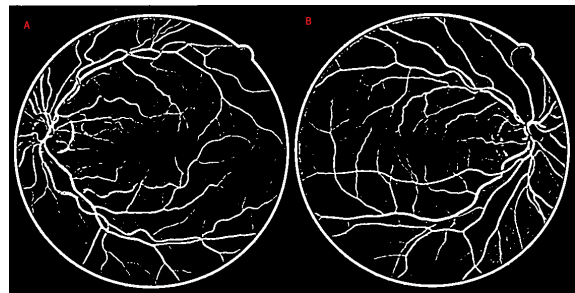


Figure 5: This picture shows the result of the execution of the algorithm on two DRIVE records. A) Segmentation of the record 01-test.tif with 0,9447 of accuracy. B) Segmentation of the record 02-test.tif with 0,9347 of accuracy.

Table 2: Table shows an overview of the performance of different methods.

Method	Accuracy
Human Observer	0.9473
Staal (Staal et al., 2004)	0.9442
Niemeijer (Niemeijer et al.,)	0.9416
Zana (Zana and Klein, 2001)	0.9377
This Study (Under development)	0.9269

processing, except the conversion from color to gray scale.

5 CONCLUSION AND DISCUSSION

Two algorithms for automatic segmentation of eye fundus images were demonstrated in this document. First, we demonstrated the successful application of wavelets on the optic disc segmentation, a fundamental process in any system of identification and classification of pathologies in retinal images. We have shown our first results and demonstrated, through the good accuracy of the firsts results, that the technique maybe applied with satisfactory accuracy. There are still problems to be solved, like the images with very low contrast on the optic disc region or with a pathologically abnormal optic disc. This problem may be addressed with the variation of the wavelets scales, or even the selection of a new type of wavelet, and the application of a adaptive filter. These testings are under development to be applied soon. An example of bad optic disc localization by the algorithm happened in the record 34 of the training group, that have a pathology and could not be properly localized and classified.

We then demonstrated the applicability of Hessian-based multi-scale filtering on segmentation of blood vessels, as well

We have successfully shown the applicability of

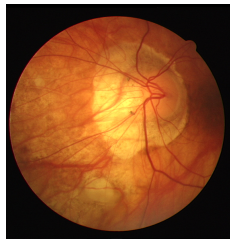


Figure 6: This picture shows an abnormal optic disc that could not yet be properly segmented by the algorithm.

these algorithms in segmentation of retinal images segmentation, as well the very good accuracy average obtained, when comparing with other studies developed on the same database.

The optic disc and the vessels are fundamental for the understanding and analysis of ocular fundus images. Our objective was to define two algorithms that will be used as a first stage in image registration to identify false positives in pathology detection and for automatic classification of detected pathologies.

ACKNOWLEDGEMENTS

The authors thank Fundo Mackenzie de Pesquisa (Mackpesquisa) from the Universidade Presbiteriana Mackenzie for the financial support for this research.

REFERENCES

- Addison, P. S. (2005). Wavelet transforms and the ECG: a review. *Physiological measurement*, 26(5):R155–99.
- Burrus, C. S., Gopinath, R. A., and Guo, H. (1998). *Introduction to Wavelets and Wavelet Transforms: A Primer*.
- Florack, L. M., ter Haar Romeny, B. M., Koenderink, J. J., and Viergever, M. a. (1992). Scale and the differential structure of images. *Image and Vision Computing*, 10(6):376–388.
- Frangi, A. F., Niessen, W. J., Vincken, K. L., and Viergever, M. A. (1998). Multiscale vessel enhancement filtering 1 Introduction 2 Method. 1496:130–137.
- Fraz, M. M., Remagnino, P., Hoppe, a., Uyyanonvara, B., Rudnicka, a. R., Owen, C. G., and Barman, S. a. (2012). Blood vessel segmentation methodologies in retinal images—a survey. *Computer methods and programs in biomedicine*, 108(1):407–33.
- Haralick, R. M. and Sternberg, S. R. (1987). Image Analysis Morphology. (4):532–550.
- Kande, G. B., Subbaiah, P. V., and Savithri, T. S. (2010). Unsupervised Fuzzy Based Vessel Segmentation In Pathological Digital Fundus Images. *J. Med. Syst.*, 34(5):849–858.
- Koenderink, J. J. (1984). Biological Cybernetics The Structure of Images. 370:363–370.
- Lupas, C. A., Tegolo, D., and Trucco, E. (2010). FABC : Retinal Vessel Segmentation Using AdaBoost. 14(5):1267–1274.
- Mallat, S. G. (1989). Theory for multiresolution signal decomposition: the wavelet representation. *IEEE Transactions on Pattern Analysis and Machine Intelligence*, 11:674–693.
- Marín, D., Aquino, A., Gegúndez-arias, M. E., and Bravo, J. M. (2010). Pr E oo f Pr E oo f. pages 1–13.
- Niemeijer, M., Staal, J., Ginneken, B. V., Loog, M., and Abr, M. D. Comparative study of retinal vessel segmentation methods on a new publicly available database.
- Ricci, E. and Perfetti, R. (2007). Retinal Blood Vessel Segmentation Using Line Operators and Support Vector Classification. *Medical Imaging, IEEE Transactions on*, 26(10):1357–1365.
- Rossant, F., Badellino, M., Chavillon, A., Bloch, I., and Paques, M. (2011). A Morphological Approach for Vessel Segmentation in Eye Fundus Images, with Quantitative Evaluation. *Journal of Medical Imaging and Health Informatics*, 1(1):42–49.
- Shapiro, L. and Stockman, G. (2001). *Computer Vision*, volume 2004.
- Sinthanayothin, C., Boyce, J. F., Cook, H. L., and Williamson, T. H. (1999). Automated localisation of the optic disc, fovea, and retinal blood vessels from digital colour fundus images. *British Journal of Ophthalmology*, 83(8):902–910.
- Staal, J., Member, A., Abràmoff, M. D., Niemeijer, M., Viergever, M. A., Ginneken, B. V., and Detection, A. R. (2004). Ridge-Based Vessel Segmentation in Color Images of the Retina. 23(4):501–509.
- Witkin, A. P. (1983). Scale-space Filtering. In *Proceedings of the Eighth International Joint Conference on Artificial Intelligence - Volume 2, IJCAI'83*, pages 1019–1022, San Francisco, CA, USA. Morgan Kaufmann Publishers Inc.
- Zana, F. and Klein, J. C. (2001). Segmentation of vessel-like patterns using mathematical morphology and curvature evaluation. *IEEE transactions on image processing : a publication of the IEEE Signal Processing Society*, 10(7):1010–9.